Feasibility of Using the Hollow Glass Microsphere to Develop Lightweight CAC-GGBFS-Blended Strain-Hardening Cementitious Composites

Wei Fan[1], Yan Zhuge[1]*, Xing Ma[1], Christopher W.K. Chow[1], Nima Gorjian[2] and Yue Liu[1]

[1]UniSA STEM, Scarce Resources and Circular Economy (ScaRCE), University of South Australia, Adelaide, SA, Australia, [2]South Australian Water Corporation, Adelaide, SA, Australia

Strain hardening cementitious composites (SHCCs) with superior tensile strength and ductility have been utilized as an effective repair material. A corrosion-resistant binder, calcium aluminate cement (CAC)–ground granulated blast-furnace slag (GGBFS) blends, has been introduced into SHCC to expand its application in the concrete sewage network rehabilitation. As a repair material, the lightweight property is particularly favorable as it can broaden its functionality. This article presents a study on developing a novel lightweight CAC-GGBFS-blended SHCC using hollow glass microsphere (HGM), namely, HGMLW-SHCCs. The fine silica sand content was substituted with HGM at 25, 50, 75, and 100 vol % in HGMLW-SHCC. We examined flowability, density, uniaxial compressive behavior, direct tensile behavior, and pseudo strain-hardening indices. Microstructure analysis was also conducted to understand the meso-scale behavior of this new lightweight composite. The newly developed HGMLW-SHCC had a 28-day density of only 1756 kg/m^3. Compressive and tensile strengths were determined in the range of 62.80–49.39 MPa and 5.81–4.19 MPa, respectively. All mixtures exhibited significant strain-hardening behavior. Even though the increased HGM content negatively affected the tensile strength of HGMLW-SHCC, it had a positive effect on its ductility. In addition, HGM can reduce crack width and tensile stress fluctuations significantly. The results showed that HGM was a promising material for producing strong and lightweight corrosion-resistant SHCCs to be used as a retrofitting material in the wastewater industry.

Keywords: strain hardening, lightweight concrete, calcium alumina cement, mechanical property, hollow glass microsphere, polyethylene fiber

Abbreviations: SHCC, strain hardening cementitious composite; HGMLW-SHCC, hollow glass microsphere incorporated lightweight SHCC; SEM, scanning electron microscopy; J_b, complementary energy; EDX, energy dispersive X-ray spectroscopy; J_{tip}, crack tip toughness; HGM, hollow glass microsphere; K_m, matrix fracture toughness; CAC, calcium aluminate cement; PSH, index of pseudo strain-hardening; GGBFS, ground granulated blast-furnace slag; E_m, Young's modulus of the matrix; PE, Polyethylene; σ_c, initial matrix cracking strength; HPMC, hydroxypropyl methyl cellulose; σ_0, fiber bridging strength; PCE, polycarboxylates; σ_{ss}, steady-state crack stress; XRD, X-ray diffraction; $\sigma_{flu-max}$, maximum stress fluctuation; XRF, X-ray fluorescence.

INTRODUCTION

Concrete sewerage pipe has been used extensively ascribed to its high strength, versatility, and cost efficiency (Song et al., 2021). However, sewerage pipes made of concrete are widely subjected to microbial-induced concrete corrosion (MICC), which causes pipe structural degradation such as mass loss, surface cracking, and reinforcement corrosion. As the sewer infrastructures are usually buried deep underground, and the traditional excavation method will cause substantial economic loss to the society; therefore, it is necessary to develop an innovative trenchless technology to repair these valuable assets.

Calcium aluminate cement (CAC)-based mortar lining has been adopted for sewerage pipe rehabilitation Two decades ago (El-Hemaly et al., 2008), the brittleness nature of the mortar material is prone to crack easily under tension load, particularly when repairing the pipe crown and invert. To improve the durability and mechanical properties of the CAC mortar lining material, the authors have taken a pilot step to tailor this material into a high performance fiber-reinforced cementitious material, namely, PE fiber-reinforced CAC-ground granulated blast-furnace slag (GGBFS)-blended strain hardening cementitious composite (SHCC) (Fan et al., 2020; Fan et al., 2020). This newly developed cementitious composite can achieve 5% tensile strain capacity with only 1% PE fiber reinforcement, with an excellent strain-hardening behavior under tension. The PE fiber-reinforced CAC-GGBFS-blended SHCC can produce multiple cracks distributed evenly with a small, tiny crack width usually less than 100 μm; this unique behavior makes it outperform the conventional cement mortar lining materials that failed from macro single cracking under tensile loading (Sheta et al., 2021). With the distinctive properties of high ductility and durability (Yu et al., 2018), SHCCs are found to be used in a broad range of applications, from repair to retrofit virgin and corroded reinforced concrete structural elements (Shang et al., 2019). As a lining material to be sprayed onto the corroded pipe wall, lightweight property will be greatly favored. However, the lightweight property of this new composite has not yet been achieved. The PE fiber-reinforced CAC-GGBFS-blended SHCC has a density of 2,140 kg/m³ while a structural lightweight concrete usually has a compressive strength over 17 MPa and a unit density less than 1920 kg/m³ (213R-14 2014). The additional load will make an adverse impact to the rehabilitated structures and limit the *in-situ* application of the repair material. Therefore, the lightweight property is greatly preferred and favored, and efforts must be made to further develop the PE fiber-reinforced CAC-GGBFS-blended SHCC with the lightweight characteristic.

A common method for producing lightweight SHCC is to incorporate lightweight aggregates. A lightweight environmental-friendly filler material, hollow glass microsphere (HGM), has been widely used as a filler material for sand replacement in cement-based composites (Wang et al., 2019; Al-Gemeel et al., 2018; Aslani and Wang 2019). HGM is a dimension-controlled hollow spherical shape particle with air encapsulated by a thin glass enclosure of sphere. The HGM material is widely available with a bulk density ranging from 120 kg/m³ to 490 kg/m³ and the

particle size is about 81 μm and less. Compared to the popular lightweight fly ash cenosphere materials, the use of HGM can offer a lower density and improve the greenness of the cementitious composite as it contains a significant amount of recycled glass (Wang et al., 2019; Meddah, 2019; Aslani et al., 2021). Hence, by replacing silica aggregates with HGM, an SHCC with more sustainable effect can be produced.

Wang and Li (2003) developed a group of lightweight SHCCs with hollow glass bubbles, expanded perlite, air bubbles, and polymeric microform. It was found that due to the relatively small size and closed-shell structure, glass bubbles were found to be the most promising lightweight filler for SHCCs by reaching an average density of 1450 kg/m³ with a high tensile strain capacity of 4.24%. Zhuge et al. (2014) replaced 10% volume of cement with HGM in fiber-reinforced cementitious composites; the compressive strength was slightly decreased with a 6% reduction of density. Al-Gemeel et al. (2018) also discovered similar results, compressive and flexural strengths were decreased, but the flowability was increased with the use of 10% volume of HGM. Chen et al. (2021) investigated HGM incorporated ultralightweight cement composites by examining their mechanical properties, durability, and the additional HGM influence on the microstructures. The results showed that the HGM incorporated lightweight composite had a density ranging from 778 to 948 kg/m³ on day-1 and a compressive strength ranging from 22.9 to 33.1 MPa at 28 days. A design concept of developing UHP-SHCC by using HGMs has been proposed by Yu et al. (2017) and Lu et al. (2021). The results indicated that the compressive strength is over 120 MPa and the air-dried density is only about 1800 kg/m³, indicating the inclusion of HGMs would be a promising material for lightweight composites. Aslani and Wang (2019) developed a lightweight fiber-reinforced cementitious composite with three different kinds of HGMs to substitute the fly ash content at 40 and 60% by weight, the density was reduced by 10% and the compressive strength was decreased by 3%. Oreshkin et al. (2016) reported that the addition of HGMs also improved the dispersion of fibers and the flowability of the mixture. Martín et al. (2021) further studied the HGM–cement paste interaction. The results showed that the HGMs can not only act as a lightweight aggregate material but also contribute as a SCM by interacting with cement initially as nucleation agents and then as pozzolanic materials. Apart from the mechanical property, the sulfuric acid resistance can also be improved with the addition of HGM (Zhang et al., 2018), which suits the need for sewerage environment.

Thus, to better utilize recycle glass resources and develop a lightweight high-performance repair material, this article first attempts to use the HGM to fully replace fine silica sand in CAC-GGBFS-blended SHCC. To optimize the mix design, different volume fractions of HGMs (V = 0, 25, 50, 75, and 100%) were added into the lightweight HGMLW-SHCC mixture. The polyethylene (PE) fiber with a low volume fraction of 1% was utilized to achieve a high tensile strain capacity. A series of experimental programs including mechanical properties and microstructure of HGMLW-SHCCs were investigated. The flowability and density of HGMLW-SHCCs were first
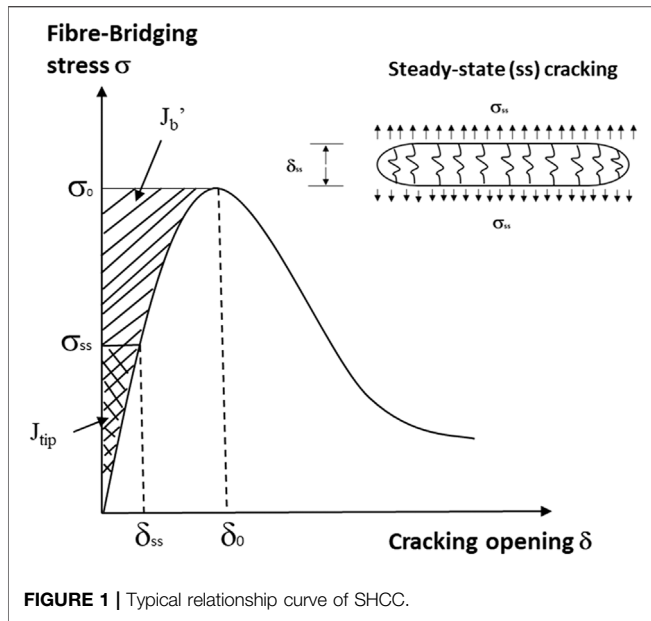
FIGURE 1 | Typical relationship curve of SHCC.

measured and followed with the compressive strength being measured at 1, 7, and 28 days. To date, research on direct tensile behavior of HGM-incorporated SHCCs is still quite limited, thus, a comprehensive tensile stress–strain relationship was investigated at 28 days after curing. The tensile strength of the lightweight HGMLW-SHCC is more than 6 MPa and its tensile strain capacity goes up to 8%. The pseudo strain-hardening (PSH) indices for all the HGMLW-SHCC mixtures were calculated to check the ductility. In addition, microstructure analysis of scanning electron microscopy (SEM) and energy dispersive X-ray spectroscopy (EDX) imaging were conducted to study the relationship between micromechanical behaviors and micromechanical performance (Liu et al., 2021).

THE MICROMECHANICS-BASED DESIGN THEORY OF THE SHCC

The design of an HGMLW-SHCC with robust tensile strain-hardening behavior relies on the understanding of micromechanical interactions between fiber, matrix, and fiber–matrix interface as the addition of HGM will increase the porosity of the CAC-GGBFS-blended cementitious matrix and lower the matrix toughness K_m. To quantify the toughness of the HGMLW-SHCC, a micromechanical-based model was used (Kanda and Li, 2002). In this analytic toolset, two PSH indices (Kanda and Li, 1998) should be verified to ensure achieving the steady propagation of multiple cracking initiated from the HGMLW-SHCC (Yu et al., 2018).

1. First, the strength index PSH_s, defined as the ratio of the fiber bridging stress σ_0 to the initial matrix cracking stress σ_c (**Figure 1**). σ_c should be lowered than σ_0. σ_c is calculated by the matrix fracture toughness K_m and preexisting internal

flaw size a_0, and σ_0 was determined based on the single-crack tensile test in *Interpretation of micromechanical analysis.*

2. Second, the energy index PSH_e, defined as the ratio of the fiber bridging complementary energy Jb' to the crack tip toughness Jtip. Jtip must be less than Jb', i.e., $J_{tip} = K_m^2/E_m \le \sigma_o \delta_o - \int_0^{\delta_o} \sigma(\delta)d\delta = J_b'$, where $\sigma(\delta)$ represents the bridging stress σ_0 versus crack opening δ curve. K_m is the fracture toughness and E_m is the elastic modulus of the matrix. E_m can be obtained from the direct tensile test and K_m can be calculated by the three-point bending test on notched beams and calculated by the following equations (Xu and Reinhardt, 1999):

$$K_m = \frac{1.5\left(F_Q + \frac{mg}{2} \times 10^{-2}\right) \times 10^{-3} \cdot S \cdot a_0^{\frac{1}{2}}}{th^2} f(\alpha),$$

$$f(\alpha) = \frac{1.99 - \alpha(1-\alpha)(2.15 - 3.93\alpha + 2.7\alpha^2)}{(1+2\alpha)(1-\alpha)^{3/2}}, \alpha = \frac{a_0}{h}.$$

F_Q is the peak load applied on the matrix; m represents the mass of the beam matrix sample; g stands for the gravitational acceleration as 9.81 m/s^2; S is span of the beam sample under the three-point bending test; a0 is the notch depth of the matrix beam sample; t and h are the width and thickness of the matrix beam sample, respectively and $f(\alpha)$ is the shape parameter of the matrix beam sample. Existing studies (Kanda and Li, 1998; Liu et al., 2021) revealed that for a polyethylene (PE) fiber-reinforced SHCC, the PSH_s value should be over 1.2 and the PSH_e value should be higher than 3 to achieve a high strain-hardening performance.

EXPERIMENTAL PROGRAM

Materials and Mix Design

HGMLW-SHCC is designed with the CAC-GGBFS-blended cementitious material, fine silica sand, HGM, water, PE fiber, and polycarboxylate-based superplasticizer; the mixture design is tabulated in **Table 1**. The mixture ID is named by the varying volume ratios of HGM to replace sand with the percentage number. HGMLW-SHCC-0 is used as a reference mixture without adding HGM, then the fine aggregate was partially replaced with HGM from 25 to 100%. Rapid hardened CAC ISTRA 40 and GGBFS were used as the binder in this study. The fine aggregates utilized in this study has a specific gravity of 2.65, the maximum grain size was 185 μm, and the mean size was 126 μm. The lightweight additive used in this study was Sphericel 110P8 HGM with a maximum grain size of 25 μm and mean size of 15 μm and an average particle density of 1,100 kg/m^3 and crushing strength of 68.95 MPa. The addition of HGM contributes to the achievement of a low density to the composites. The physical properties of Sphericel 110P8 are provided in **Table 2**. To impart the high ductility, a high fiber aspect ratio (Lf (18 mm)/df (20 μm) = 900), high tensile strength (3,000 MPa) polyethylene (PE) fiber with a volume fraction of 1% was used to increase the fiber–matrix interface area which improves the fiber bridging capacity. To maintain the flowability of the mixture, a viscosity agent hydroxypropyl

TABLE 1 | Mix design of HGMLW-SHCC (kg/m³).

Mixture ID	Binder		Filler		Water	HPMC[a]	PCE[b]	PE fiber (1% vol)	W/b
	Cement	GGBFS	Fine sand	HGM					
HGMLW-SHCC-0 (Control mix	480	720	594	0	370	0.5	1.0	10	0.3
HGMLW-SHCC-25	480	720	445	62	370	0.5	1.0	10	0.3
HGMLW-SHCC-50	480	720	296	124	370	0.5	1.0	10	0.3
HGMLW-SHCC-75	480	720	148	185	370	0.5	1.0	10	0.3
HGMLW-SHCC-100	480	720	0	246	370	0.5	1.0	10	0.3

[a]Hydroxypropyl methyl cellulose.
[b]Powder polycarboxylates superplasticizer and water to binder ratio.

TABLE 2 | Specification of HGM 110P8 powder.

Properties	HGM 110P8
Specific gravity	1.1
Bulk density (g/cm³)	0.49
Particle size distribution (μm)	2–25
Particle mean size (μm)	15
Maximum working pressure (MPa)	68.98

TABLE 3 | XRF results and loss of ignition (LOI) of ingredients.

Chemical content (wt%)	CAC (%)	GGBFS (%)	HGM (%)
CaO	37.72	45.78	5.41
SiO$_2$	4.67	32.20	54.53
Al$_2$O$_3$	37.85	12.58	< 0.01
MgO	0.48	5.34	0.452
Fe$_2$O$_3$	16.48	0.475	0.077
Na$_2$O	0.155	0.24	25.717
TiO$_2$	1.89	0.66	< 0.01
K$_2$O	0.15	0.397	0.077
Cr$_2$O$_3$	0.127	0.003	0.006
LOI[a]	0.64	2.32	3.73

[a]Loss on ignition.

methylcellulose (HPMC) and a powder type polycarboxylates (PCE) superplasticizer were both found necessary in HGMLW-SHCC mixtures for achieving adequate workability. The chemical composition of HGM, CAC, and GGBFS were quantitatively analyzed by X-Ray fluorescence (XRF) as shown in **Table 3**. In addition to the chemical element analysis, the mineral compounds were also investigated by X-ray diffraction (XRD) measurements as shown in **Figure 2A**. XRD analysis results revealed that CAC was well crystalline while HGM was completely amorphous. Gradation curves of all the ingredients are shown in **Figure 2B**. It should be noted that the flowability of mixtures was affected considerably with the increasing content of HGM.

Mixing Procedure and Specimen Preparation

It is critical to mix and make the PE fiber uniformly dispersed to achieve optimal material performances. All HGMLW-SHCC

mixtures were mixed in a Hobart mixer with 10-L capacity. The solid ingredients including the CAC, GGBFS, silica sand, and HGM were first dry mixed at the speed of 140 rpm for 1 min. Then premixed water with HPMC and PCE powder was added into the mixture and mixed at the speed of 140 rpm for 6 min then 420 rpm for 2 min until the homogenous and consistent state was achieved. PE fibers were then gradually added into the mixture and mixed at the speed of 140 rpm first until the fibers were uniformly dispersed then turned to the speed of 420 rpm for 2 min. Finally, the mixture was poured into steel molds and covered with plastic sheets. All the specimens were demolded after 24 h and then cured in air at the temperature of 23°C and relative humidity (RH) of 98% until the age of 28 days.
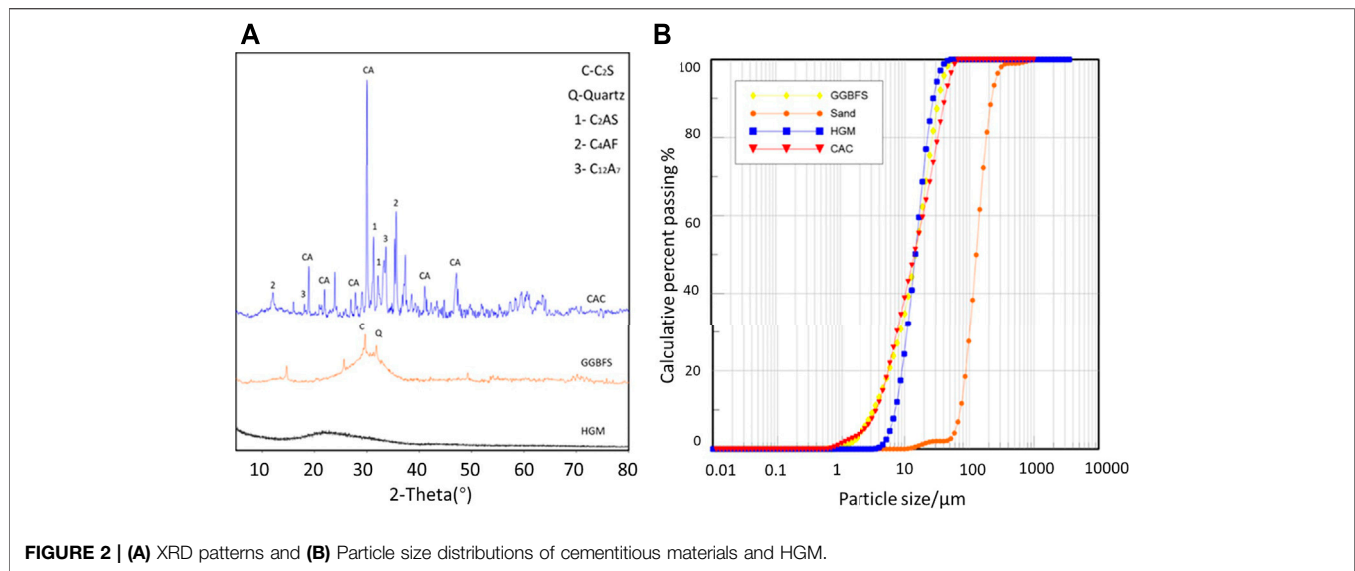
Testing Procedure
Physical Properties

The physical properties were first investigated. The flowability of the fresh HGMLW-SHCC in a different mixture design was examined with the mini-slump test, also known as spread-flow tests. A mini-slump cone was used to fill with the mortar, located in the center of the flat plate. Second, the mini-slump cone was lifted carefully in 5 seconds to allow a free spread of the mortar mixture for 3 minutes. The diameter of the spread was measured and averaged in two perpendicular directions. Then, the spread value was calculated by the subtraction of the two-average value between the diameters and the cone bottom. Details of the tests can be found in Nematollahi and Sanjayan (2014). A relative slump (T_P) can be calculated as:

$$\Gamma_P = \left(\frac{D_1}{D_0}\right)^2 - 1,$$

where D_1 is the average value of the two orthogonal diameters of the mixture and D_0 is the diameter of the cone bottom.

Apart from examining the flowability of the HGMLW-SHCC, it is also significant to avoid the damage of 110P8 HGM during mixing to provide lightweight to the composite. Therefore, harden-state density measurement was conducted to discover the damage of 110P8 HGM during mixing. The tested density was compared with the estimated value based on the specific gravity of all ingredients and mix proportions.

FIGURE 2 | (A) XRD patterns and (B) Particle size distributions of cementitious materials and HGM.

Mechanical Tests

A series of mechanical tests were conducted to evaluate the influence of HGM content on the mechanical properties of HGMLW-SHCC. The uniaxial compressive strength of HGMLW-SHCC was measured according to ASTM C109 (2008), at least three 50 mm cubes were tested at the age of 1, 7 and 28 days after curing and the mean value was recorded. The test was conducted by a load-controlled testing machine with a capacity of 1,500 kN with a load control rate of 50 kN/min under a quasi-static condition.

As recommended by the JSCE (Japan Society of Civil Engineers, 2008), dog bone–shaped specimens were used to measure the tensile behavior of HGMLW-SHCC, a constant loading rate was operated at 0.5 mm/min as a displacement control. Two linear variable displacement transducers (LVDTs) with a gauge length of 80 mm were attached on both sides of the dog-bone specimen to measure the elongation; the testing setup and specimen geometry are shown in **Figure 3**.

To discover the impact of HGM on the fracture toughness of the HGMLW-SHCC cementitious matrix, the three-point bending test was executed on $40 \times 40 \times 160$ mm^3 notched beams. Beams were prepared based on the mixture proportions but without adding the fibers. As depicted in **Figure 3B**, a 12 mm notch was cut on the bottom surface of the midspan by using a small electronic diamond saw. The test was conducted with a loading rate of 1 mm/min according to the RILEM FMC-50 method (Belysheva et al., 1990). A clip-on extensometer was installed on the lateral surface to measure the crack opening displacement as shown in **Figure 3B**.

The single-crack tensile test was performed to investigate the effect of HGM content on the fiber-bridging capacity. Dog-bone specimens were notched around the four faces in the midheight of the specimen before cutting using a saw blade (thickness of 0.4 mm) to promote the formation of a single crack after 28 days curing. The notches depth were 2

and 6.5 mm in two perpendicular directions at the cross section which is shown in **Figure 3C**. The single-crack tensile test was conducted on the same instrument as uniaxial tensile tests. The loading speed was set to 1 mm/min and the crack openings were measured by using an Instron extensometer.

Microstructure Analysis

To have a further understanding of the interaction between the PE fiber and the cementitious matrices with different HGM content, the microstructures analysis was conducted using scanning electron microscopy (SEM) and energy-dispersive X-ray spectroscopy (EDX) mapping analysis. Nail-sized samples were taken from the fractured specimen of the dog-bone specimen after the tensile test then oven-dried at 40°C for 24 h (Liu et al., 2021).
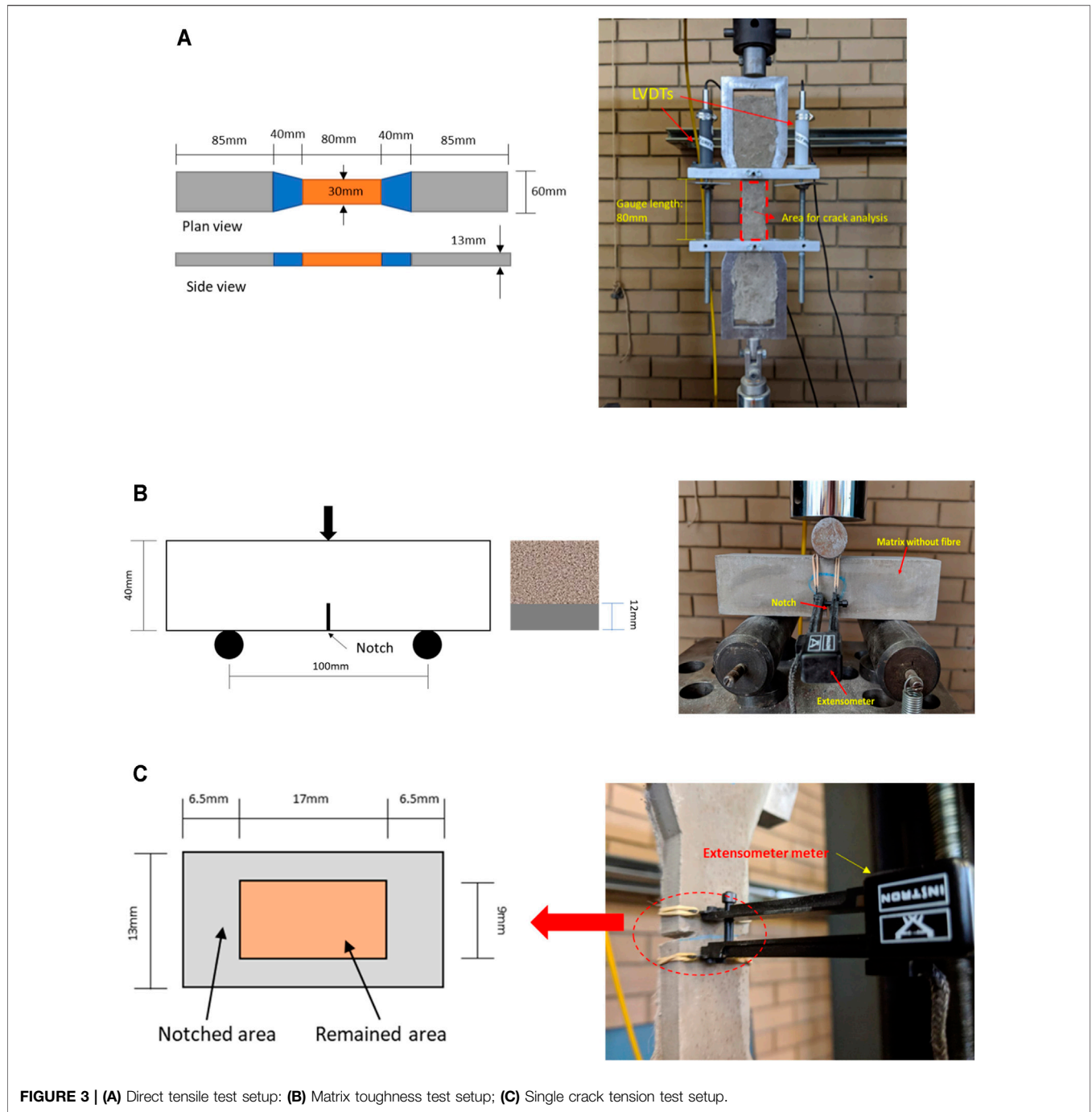
RESULTS AND DISCUSSION

Flowability

Flowability results of each fresh HGMLW-SHCC mixture are graphically presented in **Figure 4A**. The spread-flow test was characterized by a relative slump value. As expected, the relative slump value experienced a 15% increase when fine silica aggregates were 100% replaced by the lightweight HGM. These results may be ascribed to the lubricating effect of the spherical-shaped HGM particles. Neither segregation nor bleeding in the mixtures was observed, and all the mixtures showed good cohesion and homogeneity.

Density

The harden-state density of the HGMLW-SHCC is an important indicator of the HGM particle survival rate. If a certain portion of the HGM particle is broken while mixing, the harden-state density measured will be expected to achieve

FIGURE 3 | (A) Direct tensile test setup; (B) Matrix toughness test setup; (C) Single crack tension test setup.
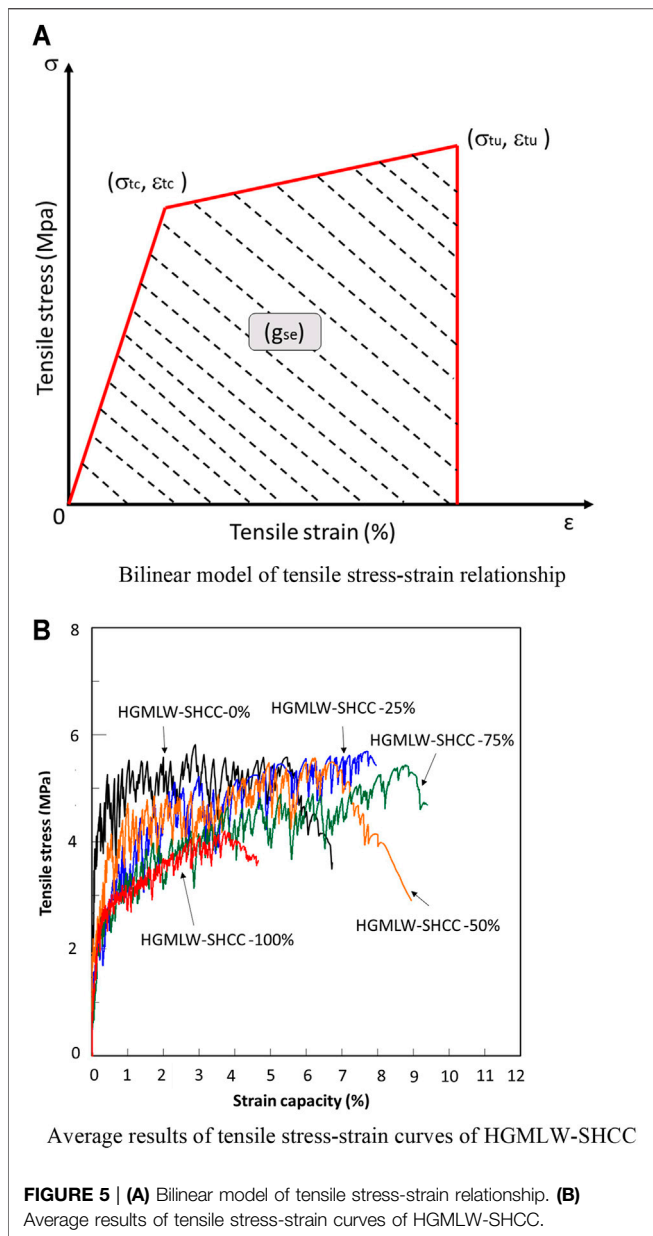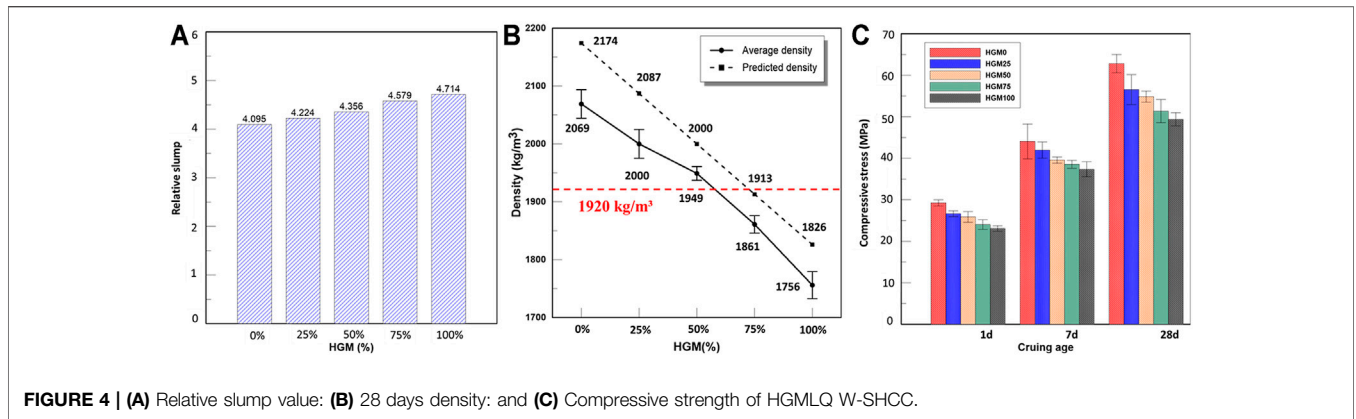
a much higher value than the targeted density estimated from the mix proportion. The harden-state density of the HGMLW-SHCC was measured after curing for 28 days; the reported density was the average of six cube samples from the same batch of mix. ACI Committee 213 recommends that density less than 1920 kg/m^3 can be referred as lightweight concrete (213R-14, 2014; Standard, 2008). The measured densities with standard deviation and theoretically calculated densities of each mixture are plotted in **Figure 4B**. Measured densities decreased with the

increasing amount of HGM. Lightweight properties were achieved when the HGM substitution rate exceeded 50%. All measured densities exhibited 3–5% lower than theoretically calculated density, which indicated that the HGMLW-SHCC was porous, and most glass balls remained unbroken.

Compressive Behavior

The average compressive strength results of HGMLW-SHCC at 1, 7, and 28 days were summarized in **Figure 4C**. CAC is known for

FIGURE 4 | (A) Relative slump value: **(B)** 28 days density: and **(C)** Compressive strength of HGMLQ W-SHCC.

Bilinear model of tensile stress-strain relationship

Average results of tensile stress-strain curves of HGMLW-SHCC

FIGURE 5 | (A) Bilinear model of tensile stress-strain relationship. **(B)** Average results of tensile stress-strain curves of HGMLW-SHCC.

rapid setting as a repair material, so it is critical to investigate the effect of the HGM content on the early strength of HGMLW-SHCC. All HGMLW-SHCC mixtures achieved over 40% of 28-day compressive strength on the first day of curing, exhibiting that HGM had a minor effect on early strength growth. Based on the compressive strength results, it can be seen that HGM degraded the composite strength as the compressive strength decreased with the increasing content of HGM. The compressive strength decreased by 10% when the HGM content was increased by 25%. The reduction trends of each curing age showed that replacing silica sand with HGM did not significantly affect the hydration process since HGM has a similar chemical composition to sand. It should be noted that HGMLW-SHCC 100 achieved a compressive strength of 49.39 MPa in 28 days; even though it is 22% less than the benchmark (control group), the strength is strong enough to be used as a repair material for concrete sewerage but adds more sustainability and durability.
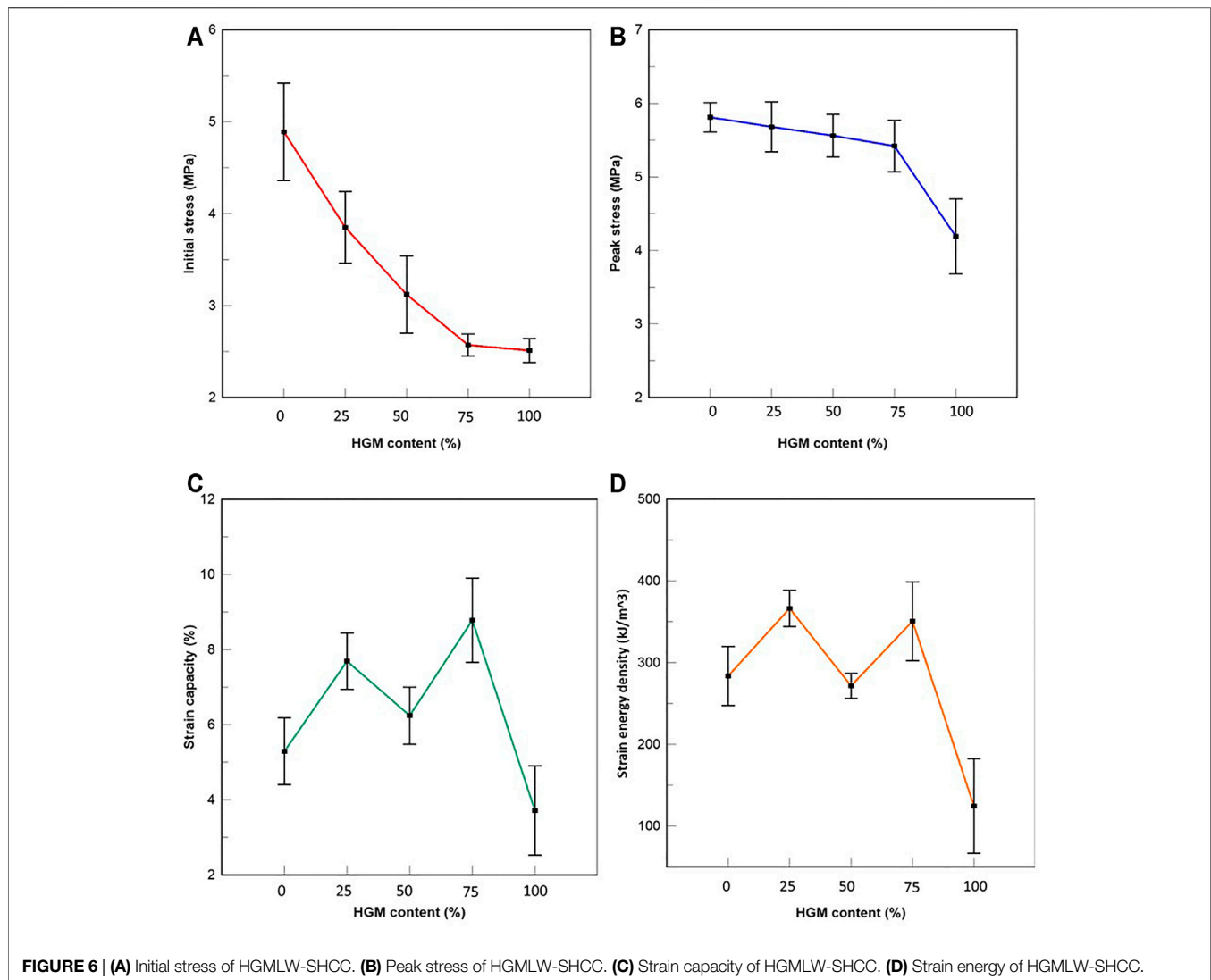
Tensile Properties
Tensile Stress–Strain Curve
To understand the failure of HGMLW-SHCC, the typical tensile stress–strain curve can be classified into three stages: start with an ascending linear stage, then a strain-hardening stage, and finally descend with a strain-softening stage. The growth of strain capacity is attributed to the increase of crack number and the crack width of SHCC remains constant during the strain-hardening process. The critical parameters representing the tensile properties of HGMLW-SHCC, including the initial cracking strength (σ_{tc}), the peak tensile strength (σ_{tu}), the strain capacity at peak stress (ε_{tu}), and the energy absorption capacity (g_{se}) are highlighted in **Figure 5A**. The strain energy density was calculated with the integral area underneath the ascending branch of the stress–strain curves as described in the formula below (Yu et al., 2020):

$$g_{se} = \int_0^{\varepsilon_{tu}} \sigma(\varepsilon)d\varepsilon.$$

The corresponding average experimental stress–strain curves of HGMLW-SHCC specimens with different HGM portions are compared in **Figure 5B**. Three specimens were tested for each

FIGURE 6 | **(A)** Initial stress of HGMLW-SHCC. **(B)** Peak stress of HGMLW-SHCC. **(C)** Strain capacity of HGMLW-SHCC. **(D)** Strain energy of HGMLW-SHCC.

mixture and an average curve was obtained and highlighted from the test results. All specimens with different mix proportions show an apparent tensile strain-hardening phenomenon. The average tensile strain of the reference mixture HGMLW-SHCC 0 achieved 5.29%. After the substitution of sand with HGM to 25, 50, 75, and 100%, the average tensile strain varied to 7.69, 6.24, 8.78, and 3.71%, respectively. The corresponding strain energy in the reference mixture HGMLW-SHCC 0 was 283.6 KJ m^{-3}. HGMLW-SHCC 25 and HGMLW-SHCC 75 achieved even higher strain energy than the reference mixture after adding HGM, with the value of 366.3 KJ m^{-3} and 350.5 KJ m^{-3}, respectively.

The four tensile parameters mentioned previuosly are presented in **Figure 6**. Similar to the compressive strength, the initial cracking stress and peak stress were decreased as the HGM substitution rate increased. The average initial cracking stress dropped about 50% from 4.89 to 2.51 MPa, while the peak stress only dropped 27% from 5.81 to 4.19 MPa when the HGM volume rate rose from 0 to 100%. It can be noted that only when the HGM

substitution rate reaches 100%, the initial stress and peak stress as well as strain capacity reduced remarkably; the tensile strain capacities of all other three mixtures with HGM addition (up to 75%) went up to an average of 6%. It can be seen that for up to 75% HGM replacement, even the peak stress was reduced slightly and the strain capacity as well as the strain energy absorption were increased. The introduction of HGM had negative impact on the stress but little effect on the tensile strain capacity, which may be attributed to the lubrication effect causing better fiber dispersion.

Crack Characteristics
The tensile properties of HGMLW-SHCC can be reflected by the cracking behavior to a certain extent. The detailed values of crack number, average crack width, and average crack spacing after unloading of HGMLW-SHCC are shown in **Figure 7A–C**. The characteristic of the cracks after failure, for e.g., the number of cracks (N_c), the average crack width (w_c), and the average crack spacing (s_c), is determined by the
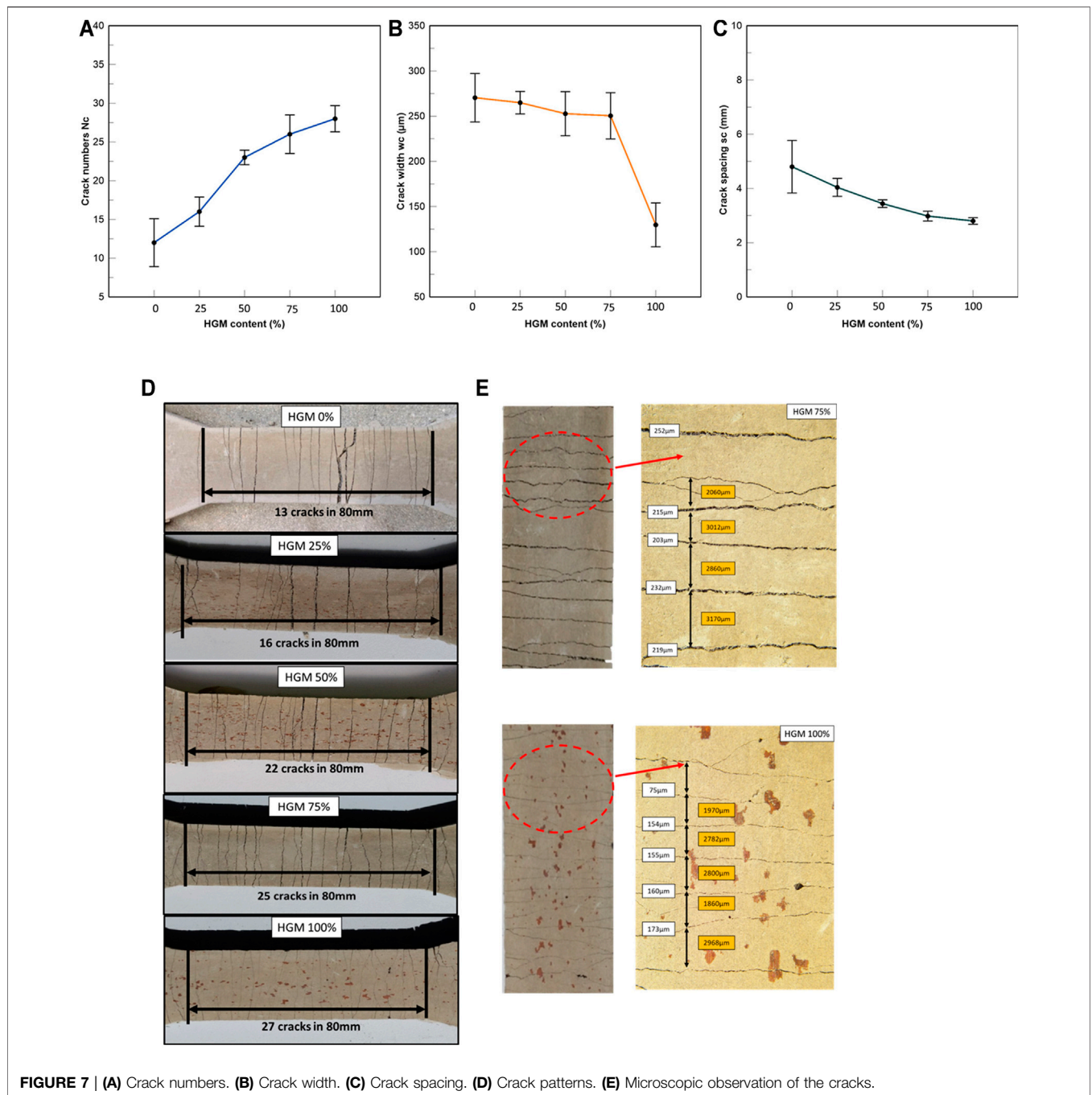
FIGURE 7 | (A) Crack numbers. **(B)** Crack width. **(C)** Crack spacing. **(D)** Crack patterns. **(E)** Microscopic observation of the cracks.

crack pattern. The number of cracks (N_c) of the specimen was counted by visually observing on both sides of the specimen. Most of the microcracks were found that went through the entire section of the specimen. The average crack width (w_c) and crack spacing were then calculated based on the formula below:

Crack width. $\delta L/Nc$

Crack spacing $= (\delta L + L)/Nc$

As shown in **Figure 7D**, all samples were shown significant multiple cracks, irrespective of the HGM amount, cracks were

saturated over the gauge length without localization. The number of cracks increased from 13 to 27 as the HGM content increased. Smaller crack widths were found when more HGM was adopted, this phenomenon is possibly owing to the better fiber dispersion behavior due to HGM as well as the spherical HGM can lessen crack propagation by reducing the tortuosity of the fracture path along the interface between the HGM and cementitious matrices. All the cracks are finely distributed with an average spacing from 2.8 to 4.8 mm. The cracking behavior of HGMLW-SHCC 75 and HGMLW-SHCC 100 were further observed under microscopic
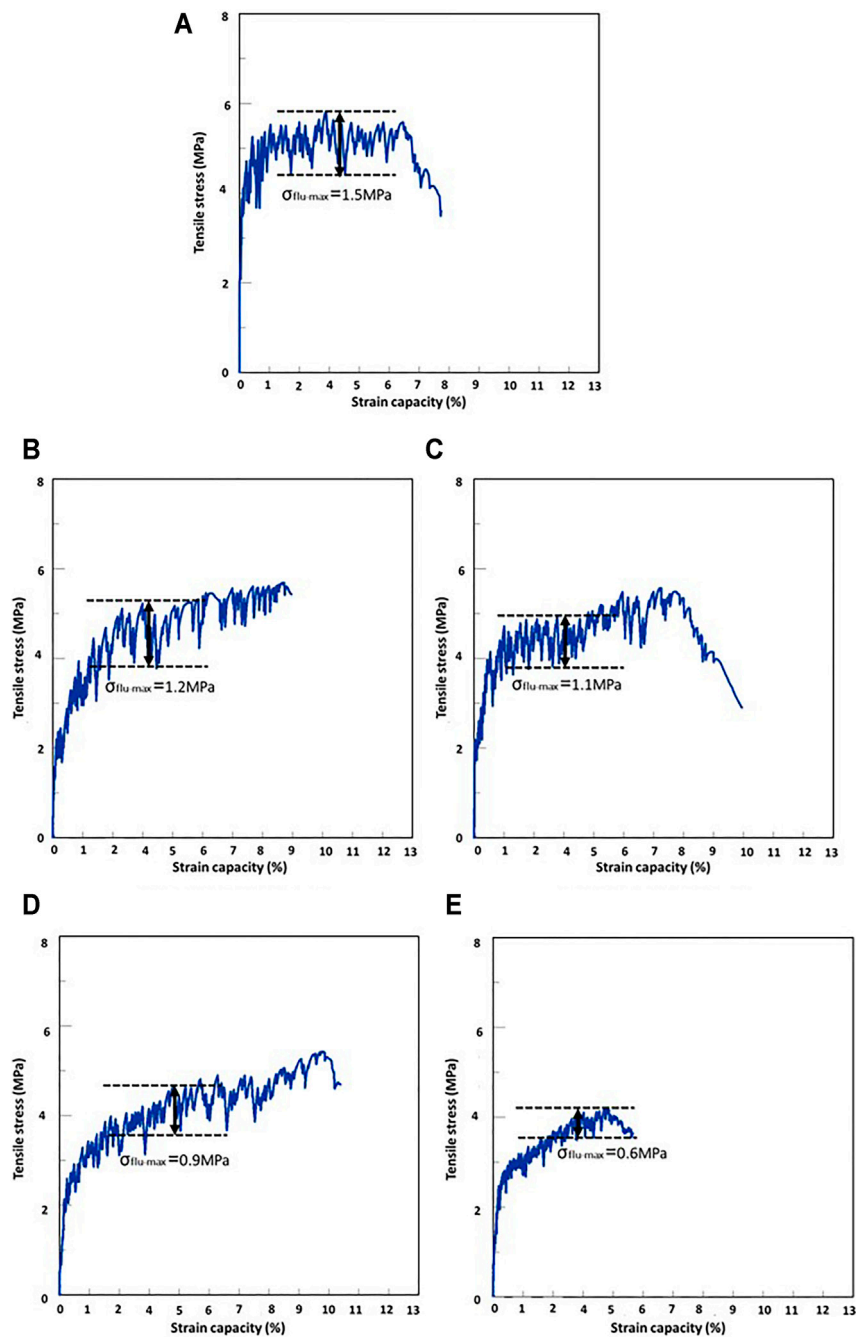
FIGURE 8 | (A) HGMLW-SHCC 0, (B) HGMLW-SHCC 25, (C) HGMLW-SHCC 50, (D) HGMLW-SHCC 75, (E) HGMLW-SHCC 100.

examination for comparison. Average crack width w_c and average crack spacing s_c were shown in **Figure 7E**. It is obvious that incorporating HGM in SHCC can effectively minimize the crack width, thus, increase the durability of the material.
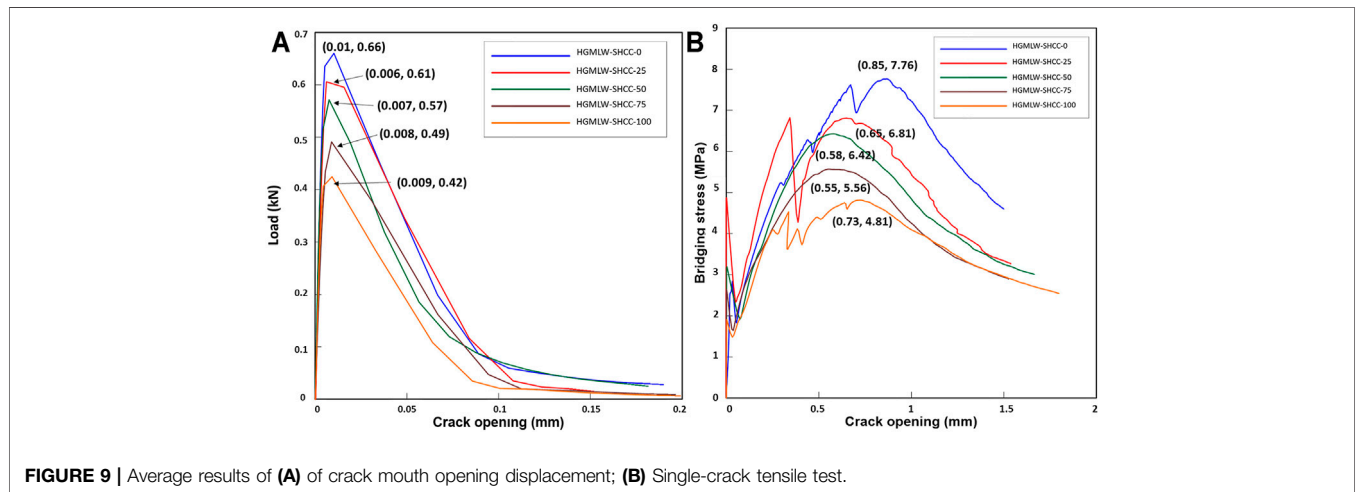
Stress Fluctuation

Much like other SHCCs, a stress fluctuation was observed under the direct tensile test during the strain-hardening part, which has negative effects on the stability of the structures. PE fiber offers great stress fluctuation due to its hydrophobicity nature, which caused the interfacial friction between the PE fibers and the cementitious matrix to be weaker during cracking. **Figure 8** shows the result of average tensile behavior of all the mixtures with the value of maximum stress fluctuations $\sigma_{flu\text{-}max}$. It can be seen that the addition of HGM can be beneficial to reduce stress fluctuation. The degree of stress fluctuation decreased as the HGM content increased, from 1.5 MPa of HGMLW-SHCC 0–0.6 MPa of HGMLW-SHCC 100. Due to the addition of

TABLE 4 | Fracture toughness of HGMLW-SHCC.

Mixture ID	Mass (kg)	F_Q (kN)	E_m (GPa)	K_m (MPa·m$^{1/2}$)	J_{tip} (J/m^2)
HGMLW-SHCC-0	0.527 ± 0.05	0.66 ± 0.25	17.56 ± 0.69	0.331 ± 0.010	12.23 ± 0.35
HGMLW-SHCC-25	0.509 ± 0.02	0.61 ± 0.18	15.40 ± 1.65	0.306 ± 0.012	9.08 ± 0.16
HGMLW-SHCC-50	0.496 ± 0.06	0.57 ± 0.03	13.48 ± 1.03	0.286 ± 0.002	9.06 ± 0.10
HGMLW-SHCC-75	0.474 ± 0.08	0.49 ± 0.16	10.28 ± 0.08	0.246 ± 0.003	6.88 ± 0.13
HGMLW-SHCC-100	0.448 ± 0.04	0.42 ± 0.08	10.04 ± 0.05	0.211 ± 0.005	5.43 ± 0.08

FIGURE 9 | Average results of **(A)** of crack mouth opening displacement; **(B)** Single-crack tensile test.

TABLE 5 | Single-crack tensile test results and PSH indices.

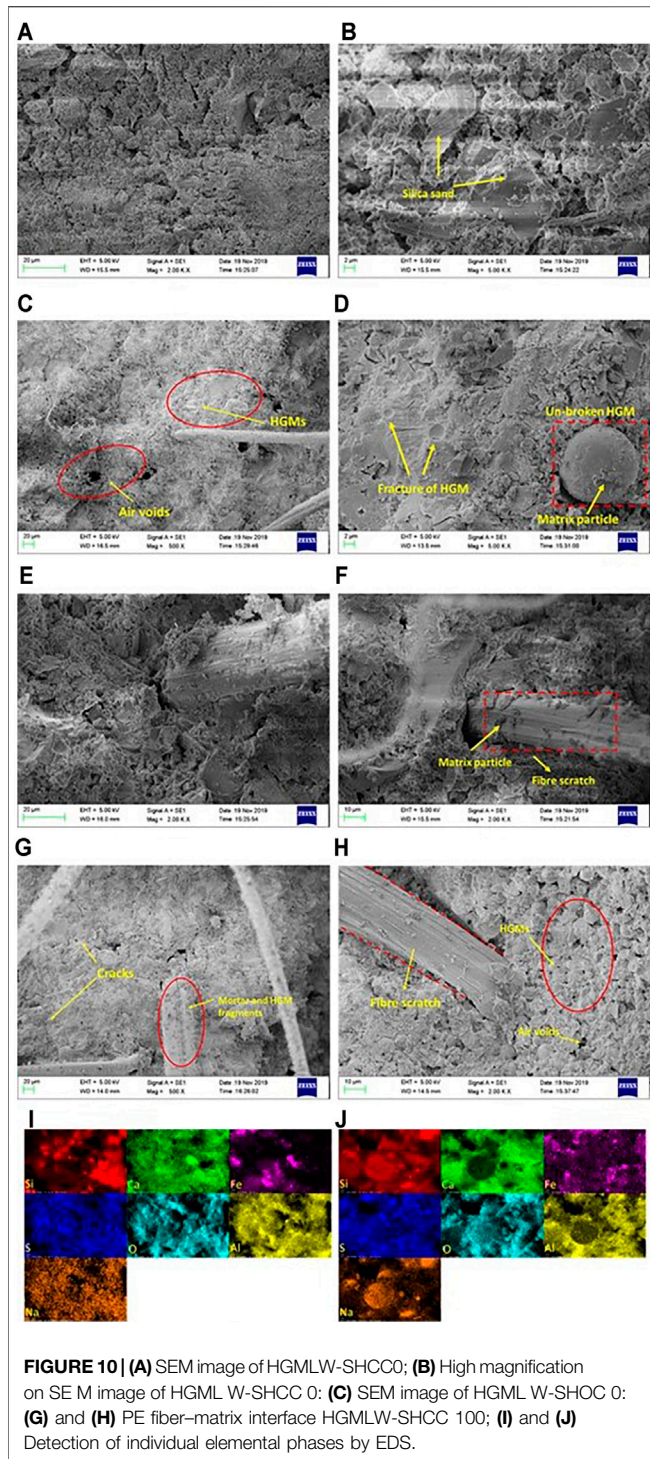| Mixture ID	HGMLW-SHCC-0	HGMLW-SHCC-25	HGMLW-SHCC-50	HGMLW-SHCC-75	HGMLW-SHCC-100
σ_0 (MPa)	7.76 ± 0.25	6.81 ± 0.13	6.42 ± 0.07	5.56 ± 0.54	4.81 ± 0.28
δ_0 (mm)	0.85 ± 0.06	0.65 ± 0.09	0.58 ± 0.12	0.55 ± 0.07	0.73 ± 0.05
J_b' (J/m^2)	1,249.2 ± 22.7	1,095.5 ± 24.3	1,032.8 ± 26.2	893.6 ± 21.5	572.3 ± 20.2
PSH$_s$ (σ_0/σ_c)	1.58 ± 0.09	1.76 ± 0.08	1.91 ± 0.06	2.05 ± 0.07	2.16 ± 0.03
PSH$_e$ (J_b'/J_{tip})	102.1 ± 3.6	120.6 ± 11.2	113.9 ± 5.1	129.8 ± 10.7	105.3 ± 3.5

HGM, the strength of the matrix reduces the small stress fluctuation caused by the interfacial stress between the PE fiber and the matrix.

Interpretation of Micromechanical Analysis

Table 4 shows the results of the matrix toughness test on the notched plain mortar beam samples. The peak load F_Q and the mass m of each sample were summarized first. The fracture toughness K_m, Young's modulus E_m, and matrix fracture energy J_{tip} were then evaluated. The peak load versus crack mouth opening displacement (CMOD) relationship was plotted in **Figure 9A**, where most of the load-displacement curves were tested with fully descending branches. The results are summarized in **Table 4**. It is obvious that the K_m and E_m decreased with the additional amount of HGM, owing to the adverse effect of HGM to the compressive strength of HGMLW-SHCC. The fracture energy J_{tip} dropped from 6.27 J/m^2 to 4.45 J/

m^2 as the introduction of HGM resulted in a lower matrix strength. The tensile stress-crack opening displacement curves of the notched HGMLW-SHCC sample results are presented in **Figure 9B**. It can be found that the peak bridging stress reduced as the HGM content increased. σ_0, δ_0, J_b', and the calculated pseudo strain-hardening (PSH$_s$ and PSH$_e$) index are listed in **Table 5**. It can be seen that the PSH$_s$ (σ_c/σ_0) value increased from 1.58 to 2.16 when the HGM replacement rate increased from 0 to 100%; this is due to the reduction in matrix cracking strength. All the mixtures showed a PSH$_s$ value larger than 1.2, which is corresponding to the steadily initiated cracks on the HGMLW-SHCC samples. Then, the PSH$_e$ (J_b'/J_{tip}) was calculated based on the complementary energy J_b' and the matrix fracture energy J_{tip}.

All mixtures showed a relatively high PSH$_e$ value, even with 100% HGM replacement. The PSH$_e$ value of HGMLW-SHCC 100 is more than 35 times higher than the

FIGURE 10 | (A) SEM image of HGMLW-SHCC0; **(B)** High magnification on SE M image of HGML W-SHCC 0: **(C)** SEM image of HGML W-SHOC 0: **(G)** and **(H)** PE fiber–matrix interface HGMLW-SHCC 100; **(I)** and **(J)** Detection of individual elemental phases by EDS.

recommended threshold value of 3 (Kanda and Li, 2002); therefore, the criterion of energy is compiled as well as a significant strain-hardening behavior was achieved.

SEM-EDX Mapping

Figure 10A–D shows the SEM images of HGMLW-SHCC. For comparison, two specimens with 0 and 100% volume fractions

of HGM were tested. **Figure 10A** indicates that the HGMLW-SHCC 0 mixture is dense and homogeneous, and no apparent air voids were observed. **Figure 10C** shows some air voids on the surface of the mortar. The number of air voids increased with increasing HGM content. These results indicate that the spherical particles of HGM induced more air voids in the matrix, which benefit the lightweight property of the end product. **Figure 10D** captured the smooth spherical shape of unbroken HGM with some attached pastes, attributing to a slight degree of pozzolanic reaction. Please note that HGM or silica sand was identified based on EDS mapping analysis (see **Figure 10I,J**).

Figure 10E–H shows the interaction of the PE fiber with blended cementitious matrix in samples of HGMLW-SHCC 0 and HGMLW-SHCC 100. **Figure 10E,F** showed that HGMLW-SHCC 0 has some residual mortar paste left on the surface of the PE fiber, indicating a good bonding strength between the PE fiber and HGMLW-SHCC 0 matrix. **Figure 10G,H** showed a relatively clean and smooth surface of PE fibers in HGMLW-SHCC 100, which may result from a weak fiber–matrix bond. These results could be attributed to the fact that the introduction of HGM into the cementitious matrix loosens the surrounding matrix, as shown in **Figure 10H**.

Figure 10I,J compare the exact distribution of various elemental phases in the samples with or without HGM addition. The elemental mapping results indicated that the calcium from hydration products was homogeneously distributed throughout the selected region in **Figure 10I**. Whereas **Figure 10J** shows the mapped region assigned to the HGM particle was rich in Si and Na, and the absence of Ca revealed that the HGM remained unreacted in the cementitious composite.

CONCLUSION

This experimental study took a pilot step to develop a lightweight SHCC by using HGM. Based on the theory of micromechanics, HGMLW-SHCC with significant strain-hardening behavior was developed. A series of mechanical and microstructural tests were conducted and the results can be summarized as follows:

1. The introduction of HGM to the PE fiber-reinforced CAC-GGBFS-blended SHCC improves the flowability and greatly reduces the density from 2069 kg/m^3 to 1756 kg/m^3, meets the requirement of lightweight concrete.
2. The compressive strength of HGMLW-SHCC reduced after adding HGM but it still achieved almost 50 MPa when fully replaced for sand. All mixtures exhibited significant strain-hardening behavior with a maximum strain capacity up to 8.78%, almost 50% higher than the reference mixture group. Tensile strength was reduced insignificantly even the HGM content increased up to 75%; tensile stress fluctuations as well as crack width were all benefited.
3. Both PSH$_s$ and PSH$_e$ indices of the designed HGMLW-SHCC have fully satisfied the recommended values in the relevant

literature, which ensures a high strain-hardening behavior of HGMLW-SHCC.

4. SEM images captured the smooth spherical shape of unbroken HGM particles. HGM shell remains intact with CAC-GGBFSA-blended matrix after 28 days of moist curing, which means that little or no interaction between the microspheres and the cementitious matrix. EDX element mapping analysis further proves HGM remained unreacted in the cementitious composite.

DATA AVAILABILITY STATEMENT

The raw data supporting the conclusions of this article will be made available by the authors, without undue reservation.

AUTHOR CONTRIBUTIONS

FW performed the data curation, formal analysis, methodology, and wrote the first draft. YZ contributed to conception and design and supervision. YL contributed to the microstructure analysis. All authors contributed to manuscript revision, read, and approved the submitted version.

ACKNOWLEDGMENTS

REFERENCES

213R-14, ACI (2014). Guide for Structural Lightweight-Aggregate Concrete, ACI COMMITTEE REPORT. Available at http://www.uomisan.edu.iq/library/admin/book/68340626265.pdf.

Al-Gemeel, A. N., Zhuge, Y., and Youssf, O. (2018). Use of Hollow Glass Microspheres and Hybrid Fibres to Improve the Mechanical Properties of Engineered Cementitious Composite. *Construction Building Mater.* 171, 858–870. doi:10.1016/j.conbuildmat.2018.03.172

Aslani, F., and Wang, L. (2019). Development of Strain-Hardening Lightweight Engineered Cementitious Composites Using Hollow Glass Microspheres. *Struct. Concrete* (April), 1–16. doi:10.1002/suco.201900096

Aslani, F., Dehghani, A., and Wang, L. (2021). The Effect of Hollow Glass Microspheres, Carbon Nanofibers and Activated Carbon Powder on Mechanical and Dry Shrinkage Performance of Ultra-lightweight Engineered Cementitious Composites. *Construction Building Mater.* 280, 122415. doi:10.1016/j.conbuildmat.2021.122415

Belysheva, G. V., Egorochkin, A. N., Sennikov, P. G., Lopatin, M. A., and Voronenkov, V. V. (1990). UV-spectroscopic Study of Complex Formation by Certain Cycloolefins with Tetracyanoethylene and Molecular Iodine. *Russ. Chem. Bull.* 39 (6), 1181–1184. doi:10.1007/bf00962380

Chen, F., Cheng, S., Zhang, G., Chen, S., and Yang, R. (2021). Development of Ultralightweight Cement Composites with Low Density and High-specific Strength Using Hollow Glass Microspheres. *J. Mater. Civil Eng.* 33 (6), 1–9. doi:10.1061/(asce)mt.1943-5533.0003739

El-Hemaly, S. A. S., Abdallah, H. A. M., Abadir, M. F., and El Sersy, H. H. (2008). Evaluation of the Internal High Alumina Cement Mortar Lining of Ductile Cast Iron Pipes Used in Sewage Transportation. *Mater. Des.* 29 (6), 1280–1283. doi:10.1016/j.matdes.2007.05.001

Fan, W., Zhuge, Y., Ma, X., Chow, C. W. K., Gorjian, N., Oh, J.-A., et al. (2020). Durability of Fibre-Reinforced Calcium Aluminate Cement (CAC)-Ground Granulated Blast Furnace Slag (GGBFS) Blended Mortar after Sulfuric Acid Attack. *Materials* 13 (17), 3822. doi:10.3390/ma13173822

Fan, W., Zhuge, Y., Ma, X., Chow, C. W. K., and Gorjian, N. (2020). Strain Hardening Behaviour of PE Fibre Reinforced Calcium Aluminate Cement (CAC) - Ground Granulated Blast Furnace (GGBFS) Blended Mortar. *Construction Building Mater.* 241, 118100. doi:10.1016/j.conbuildmat.2020.118100

JapanSociety of Civil Engineers (2008) Recommendations for Design and Construction of High Performance Fiber Reinforced Cement Composites with Multiple Fine Cracks (HPFRCC). *Concrete Engineering Ser* 82, 6–10.

Testing MethodAvailable at http://www.jsce.or.jp/committee/concrete/e/index.html

Kanda, T., and Li, V. C. (1998). Multiple Cracking Sequence and Saturation in Fiber Reinforced Cementitious Composites. *Concrete Res. Tech.* 9(2), 19–33. doi:10.3151/crt1990.9.2_19

Kanda, T., and Li, V. C. (2002). New Micromechanics Design Theory for Pseudostrain Hardening Cementitious Composite. *J. Eng. Mech.* 125 (4), 373–381. doi:10.1061/(asce)0733-9399(1999)125:4(373)

Liu, Y., Zhuge, Y., Chow, C. W. K., Keegan, A., Ma, J., Hall, C., et al. (2021). Cementitious Composites Containing Alum Sludge Ash: An Investigation of Microstructural Features by an Advanced Nanoindentation Technology. *Construction Building Mater.* 299 (July), 124286. doi:10.1016/j.conbuildmat.2021.124286

Liu, Y., Zhuge, Y., Chow, C. W. K., Keegan, A., Pham, P. N., Li, D., et al. (2021). The Potential Use of Drinking Water Sludge Ash as Supplementary Cementitious Material in the Manufacture of Concrete Blocks. *Resour. Conservation Recycling* 168, 105291. doi:10.1016/j.resconrec.2020.105291

Lu, J.-X., Shen, P., Zheng, H., Ali, H. A., and Poon, C. S. (2021). Development and Characteristics of Ultra High-Performance Lightweight Cementitious Composites (UHP-LCCs). *Cement Concrete Res.* 145 (September 2020), 106462. doi:10.1016/j.cemconres.2021.106462

Martín, C. M., Scarponi, N. B., Villagrán, Y. A., Manzanal, D. G., and Piqué, T. M. (2021). Pozzolanic Activity Quantification of Hollow Glass Microspheres. *Cement and Concrete Composites* 118 (February)103981. doi:10.1016/j.cemconcomp.2021.103981

Nematollahi, B., and Sanjayan, J. (2014). Effect of Different Superplasticizers and Activator Combinations on Workability and Strength of Fly Ash Based Geopolymer. *Mater. Des.* 57, 667–672. doi:10.1016/j.matdes.2014.01.064

Oreshkin, D., Semenov, V., and Rozovskaya, T. (2016). Properties of Light-Weight Extruded Concrete with Hollow Glass Microspheres. *Proced. Eng.* 153, 638–643. doi:10.1016/j.proeng.2016.08.214

Seddik Meddah, M. (2019).Use of Waste Window Glass as Substitute of Natural Sand in Concrete Production, *IOP Conf. Ser. Mater. Sci. Eng.* 603 3 IOP Publishing, 032011. doi:10.1088/1757-899X/603/3/032011

Shang, X. Y., Jiang, T., Li, L. Z., and Zhou, D. (2019). Strengthening of RC Structures by Using Engineered Cementitious Composites: A Review. *Sustainability (Switzerland)* 11 (12). doi:10.3390/su11123384

Sheta, A., Ma, X., Zhuge, Y., ElGawady, M. A., Mills, J. E., Singh, A., et al. (2021). Structural Performance of Novel Thin-Walled Composite Cold-Formed Steel/PE-ECC Beams. *Thin-Walled Structures* 162 (February), 107586. doi:10.1016/j.tws.2021.107586

Song, Y., Chetty, K., Garbe, U., Wei, J., Bu, H., O'moore, L., et al. (2021). A Novel Granular Sludge-Based and Highly Corrosion-Resistant Bio-Concrete in Sewers. *Sci. Total Environ.* 791, 148270. doi:10.1016/j.scitotenv.2021.148270

Standard, A. S. T. M. (2008). *ASTM C109-Standard Test Method for Compressive Strength of Hydraulic Cement Mortars.* West Conshohocken, PA,US: " ASTM International

Wang, L., Aslani, F., Hajirasouliha, I., and Roquino, E. (2019). Ultra-Lightweight Engineered Cementitious Composite Using Waste Recycled Hollow Glass Microspheres. *J. Clean. Prod.* 33(6) 119331. doi:10.1016/j.jclepro.2019.119331

Wang, S., and Li, V. C. (2003), 27 Lightweight Engineered Cementitious Composites (ECC). In PRO 30: 4th International RILEM Workshop on High Performance Fiber Reinforced Cement Composites (HPFRCC 4), Michigan: RILEM Publications, 379

Xu, S., and Reinhardt, H. W. (1999). Determination of Double-K Criterion for Crack Propagation in Quasi-Brittle Fracture Part II: Analytical Evaluating and Practical Measuring Methods for Three-Point Bending Notched Beams. *Int. J. Fracture* 98 (2), 151–177. Available at: http://link.springer.com/article/10.1023/A:1018740728458. doi:10.1023/a:1018740728458

Yu, K.-Q., Yu, J.-T., Dai, J.-G., Lu, Z.-D., and Shah, S. P. (2018). Development of Ultra-high Performance Engineered Cementitious Composites Using Polyethylene (PE) Fibers. *Construction Building Mater.* 158, 217–227. doi:10.1016/j.conbuildmat.2017.10.040

Yu, K., Ding, Y., Liu, J., and Bai, Y. (2020). Energy Dissipation Characteristics of All-Grade Polyethylene Fiber-Reinforced Engineered Cementitious Composites (PE-ECC). *Cement and Concrete Composites* 106 (October 2019), 103459. doi:10.1016/j.cemconcomp.2019.103459

Yu, K., Wang, Y., Yu, J., and Xu, S. (2017). A Strain-Hardening Cementitious Composites with the Tensile Capacity up to 8 %. *Construction Building Mater.* 137, 410–419. doi:10.1016/j.conbuildmat.2017.01.060

Yu, K., Li, L., Yu, J., Xiao, J., Ye, J., and Wang, Y. (2018). Feasibility of Using Ultra-high Ductility Cementitious Composites for Concrete Structures without Steel Rebar. *Eng. Structures* 170, 11–20. doi:10.1016/j.engstruct.2018.05.037

Zhang, W., Yao, X., Yang, T., Liu, C., and Zhang, Z. (2018). Increasing Mechanical Strength and Acid Resistance of Geopolymers by Incorporating Different Siliceous Materials. *Construction Building Mater.* 175, 411–421. doi:10.1016/j.conbuildmat.2018.03.195

Zhuge, Yan., Shen, C. J., Lu, G. X., Hesse, G., Chen, S., and Ruan, D. (2014). "Material Properties and Impact Resistance of a New Lightweight Engineered Cementitious Composite," in In: 23rd Australasian Conference on the Mechanics of Structures and Materials (ACMSM 23), Byron Bay, Australia, Dec 2014, 9–12.